Soft Matter

PAPER

View Article Online
View Journal | View Issue

Cite this: *Soft Matter*, 2022, **18**, 6618

Zwitterionic surface chemistry enhances detachment of bacteria under shear†

Molly K. Shave,[ab] Yitian Zhou,[ab] Jiwon Kim,[ac] Ye Chan Kim,[b] Jaime Hutchison,[d] Denis Bendejacq,[d] Mark Goulian,[e] Jonghoon Choi,[ac] Russell J. Composto *[ab] and Daeyeon Lee *[a]

The ubiquitous nature of microorganisms, especially of biofilm-forming bacteria, makes biofouling a prevalent challenge in many settings, including medical and industrial environments immersed in liquid and subjected to shear forces. Recent studies have shown that zwitterionic groups are effective in suppressing bacteria and protein adhesion as well as biofilm growth. However, the effect of zwitterionic groups on the removal of surface-bound bacteria has not been extensively studied. Here we present a microfluidic approach to evaluate the effectiveness in facilitating bacteria detachment by shear of an antifouling surface treatment using (3-(dimethyl;(3-trimethoxysilyl)propyl)ammonia propane-1-sulfonate), a sulfobetaine silane (SBS). Control studies show that SBS-functionalized surfaces greatly increase protein (bovine serum albumin) removal upon rinsing. On the same surfaces, enhanced bacteria (*Pseudomonas aeruginosa*) removal is observed under shear. To quantify this enhancement a microfluidic shear device is employed to investigate how SBS-functionalized surfaces promote bacteria detachment under shear. By using a microfluidic channel with five shear zones, we compare the removal of bacteria from zwitterionic and glass surfaces under different shear rates. At times of 15 min, 30 min, and 60 min, bacteria adhesion on SBS-functionalized surfaces is reduced relative to the control surface (glass) under quiescent conditions. However, surface-associated bacteria on the SBS-functionalized glass and control show similar percentages of live cells, suggesting minimal intrinsic biocidal effect from the SBS-functionalized surface. Notably, when exposed to shear rates ranging from 10^4 to 10^5 s^{-1}, significantly fewer bacteria remain on the SBS-functionalized surfaces. These results demonstrate the potential of zwitterionic sulfobetaine as effective antifouling coatings that facilitate the removal of bacteria under shear.

Received 12th January 2022,
Accepted 26th July 2022

DOI: 10.1039/d2sm00065b

rsc.li/soft-matter-journal

Introduction

Bacteria are present everywhere from the deepest parts of the ocean, to various surfaces we come in contact within our daily routine.[1] Many of these bacteria move on and off or between surfaces as they adapt to their environment.[2] To survive, bacteria colonize these surfaces and form biofilms which are complex collections of microbes and extracellular polymeric substances (EPS).[3] While these biofilms can be beneficial for the survival of the bacteria, they can have extremely costly[4] and deadly consequences.[5] For example, it is estimated that biofilm formation on ship hulls contributes an additional 30–50% in fuel costs, which is 1.6–4% of the operational costs of the ship.[6,7] Biofilm growth in cooling towers can cause significant reductions in efficiencies, necessitating the removal of the biofilm using physical methods or biocides, but some of these biocides can be environmentally toxic.[8] In medical settings, hospital-associated infections that are often caused by biofilms lead to substantial morbidity and deaths, in addition to higher costs in health care spending.[9,10]

Negative impacts associated with biofilms have motivated the development of surface coatings and treatments that are designed to prevent or eliminate biofilms. These coatings generally fall into two categories: biocidal coatings designed to release antibacterial agents,[11,12] which can kill the bacteria and prevent biofilm formation, and anti-fouling coatings designed to prevent bacteria from adhering or stay adhered to

[a] *Department of Chemical and Biomolecular Engineering, University of Pennsylvania, Philadelphia, PA, 19104, USA. E-mail: composto@seas.upenn.edu, daeyeon@seas.upenn.edu*
[b] *Department of Materials Science and Engineering, University of Pennsylvania, Philadelphia, PA, 19104, USA*
[c] *School of Integrative Engineering, Chung-Ang University, Seoul, 06974, Republic of Korea*
[d] *Solvay, Bristol, PA, USA*
[e] *Department of Biology, University of Pennsylvania, Philadelphia, PA, 19104, USA*

† Electronic supplementary information (ESI) available. See DOI: https://doi.org/10.1039/d2sm00065b

the surface.[13–15] Methods to prevent surface adhesion include steric repulsion,[16] surface topography,[17] low surface energy[18] and electrostatic repulsion.[19] These bacteria adhesion-resistant coatings are favored over the biocide-based methods in many cases due to the development of resistance of bacteria to biocides[20] and the tendency of dead bacteria to accumulate on antibacterial surfaces leading to ineffectiveness of the coating.[21]

A number of different antifouling surfaces including poly-(ethylene glycol) (PEG) and hydrogels have been developed.[22] More recently, surface grafted zwitterionic functional groups such as sulfobetaine have shown superb anti-fouling capabilities preventing adhesion of proteins (*e.g.*, fibrinogen[23]), attachment of bacteria and growth of biofilms, potentially due to their strong interactions and association with water molecules. The degree of surface packing of these sulfobetaines to prevent bacterial adhesion and growth has an important effect as well as the hydration characteristics of their group itself.[24] Despite these promising results, bacteria are extremely apt at colonizing surfaces, including antifouling surfaces, which could happen due to imperfection in the coatings or bacteria's ability to secrete highly adhesive EPS. Moreover, as some of the antifouling coating undergoes desorption and degradation over time, biofilm resistance may be lost in these more passive strategies that are repelling bacteria through physiochemical properties.[25,26]

Biofilm growth occurs in multiple stages. Initially, bacteria that encounter the surface attach reversibly and are able to adhere or leave the surface. Eventually, bacteria adsorb more avidly and begin to produce a polymeric extracellular matrix which subsequently leads to microcolony formation. These microcolonies can then mature into complete biofilms and eventually develop to a state that they can disperse single cell bacteria to restart the process.[27] Our work focuses on understanding the effect of surface zwitterionic functional groups on bacteria adhesion and, more importantly, their removal under flow in the initial stages involving reversible/irreversible adhesion, microcolony formation and early biofilm formation. During these early stages of biofilm development, bacteria are less recalcitrant to many external stresses and antibacterial agents.[28] Therefore, it is highly desirable to develop surface treatments that facilitate removal of bacteria or microcolonies during the early stages of biofilm formation, before they fully mature and differentiate into highly robust biofilms.

Conventionally, mechanical[29,30] as well as chemical disruptions[31] have been used to remove bacteria and biofilms from the surface, which may not be practical for a number of situations, especially those involving surfaces that are not easily accessible or are associated with clinical settings such as catheters and implanted medical devices. Interestingly there are few studies that focus on the removal of bacteria from the surface before they develop into robust biofilms using simple methods such high shear,[32,33] and pH change.[34]

In this work, we investigate the removal of bacteria in the early stages of biofilm formation from a zwitterionic group-functionalized surface using a simple shear in a microfluidic device. Unlike conventional biofilm testing methods such as the CDC bioreactor[35] that require long time, large volumes of materials and are difficult to directly observe bacteria-surface interactions, microfluidic devices use significantly less materials, potentially enabling rapid screening. Moreover, it is possible to precisely control the shear over the surface, enabling quantitative analysis of the effect of flow on bacteria adhesion and removal. While previous studies have focused on the effect of surface-grafted zwitterionic on protein adhesion, bacteria attachment and biofilm growth, the novelty of this work is the demonstration of facile removal of bacteria from the zwitterion group grafted surface under a simple shear flow. We show that although bacteria are able to adhere and populate on a zwitterionic group-functionalized surface, even low shear can effectively remove a significant number of bacteria from the surface, whereas bacteria on a glass surface are highly resistant to removal under the same condition. Our work sheds insight into an important aspect of biofilm managements and prevention by raising the possibility of designing surfaces that are able to enable easy removal of bacteria in their early stages of biofilm formation.

Materials and methods

Materials

Zwitterionic silane (3-(dimethyl;(3-trimethoxysilyl)propyl)ammonia propane-1-sulfonate) (a sulfobetaine silane, or SBS) is purchased from Gelest (Morrisville, PA) and used as received. Bovine Serum Albumin (BSA, A3059) is purchased from Sigma Aldrich (St. Louis, MO) and used as received. 10× phosphate buffered saline (PBS) solution is purchased from Sigma Aldrich and diluted to 1× working concentration using MilliQ Water. All other materials are used as received.

Bacteria culture

The *P. aeruginosa* PAO1 used in this study is purchased from the PAO1 transposon mutant library.[36] The bacteria are stored in LB-glycerol frozen stocks at −80 °C. For use, bacteria are streaked onto LB Agar plates (Carolina Biosupplies) and grown overnight at 37 °C. Plates are sealed with parafilm and stored at 4 °C for no longer than 1 week. Single bacterial cultures are then grown in 10 mL LB Media (Carolina Biosupplies) for 16 hours at 37 °C and 250 rpm. Immediately prior to use 0.5 mL of overnight culture is diluted in 10 mL fresh LB Media, preheated to a temperature of 37 °C.

Characterization of zwitterionic surface functionalization and protein adhesion

The adsorption of SBS onto silica coated crystals and protein adsorption experiments are completed using a QSense Analyzer E4 from Biolin Scientific (Gothenburg, Sweden) coupled to an IPC microprocessor controlled dispensing pump from ISMATEC (Wertheim, Germany) for a flow cell set up. Initial baselines are taken in DI water and 1× PBS. For SBS adsorption experiments 10 mg mL^{-1} SBS is flowed over crystal at a 50 μL min^{-1} flow rate until frequency stabilized and a DI water rinse

is followed until frequency stabilizes again. For S experiments 1 mg mL^{-1} BSA in 1× PBS is flowed over SBS coated and uncoated crystals until frequency stabilized followed by rinsing.

The thickness of the grafted SBS is characterized by an Alpha-SE Ellipsometer from J. A. Woollam (Lincoln, NE). The measurements are performed using a white light beam at an incident angle of 70° degrees, in the wavelength range of 380 to 900 nm. The thickness of SBS layer is analyzed using the CompleteEASE software package provided by J.A. Woollam using the Cauchy model. For ellipsometry modeling, the Cauchy model is expressed as: $n(\lambda) = A + B/\lambda^2 + C/\lambda^4$; $k(\lambda) = 0$, where A, B and C are optical constants, λ is the wavelength (μm), n and k are the real and imaginary components of the index of refraction. For this study, $A = 1.5$ and $B = C = 0$ are assumed. Each sample is measured three times and averaged. A Dimension Icon atomic force microscope (AFM) from Bruker (Billerica, MA) is used to characterize the surface topography of SBS-functionalized surfaces. It is used in tapping mode with AFM probes (HQ:NSC15/Al BS) which have a resonance frequency of 325 kHz, a force constant of 40 N m^{-1}, and a radius of 8 nm. The scan area is 1 μm × 1 μm for all images. Gwyddion software is used to identify and quantitatively analyze the surface and roughness of the sample. For image scanning, scan rate, integral gain, proportional gain, and amplitude setpoint are set to 1.00 Hz, 1.20, 6.00, and 500 mV, respectively. R_q (root mean square roughness) is obtained in nine random spots for each sample and averaged. A silicon wafer is functionalized in a 10 mg mL^{-1} SBS aqueous solution for 2 h with gentle shaking. After grafting, the SBS-functionalized wafer is washed with DI water, IPA and dried with nitrogen.

Microfluidic device fabrication

The microfluidic channel is designed using Autodesk AutoCAD software, and a film photomask of the design is purchased from CAD/Art Services (Bandon, OR) at 20 000 dpi resolution. Master for the microfluidic device is prepared using soft lithography techniques and KMPR 1050 negative photoresist. This channel has five different shear zones, and the shear rate is calculated using:

$$\dot{\gamma} = \frac{6Q}{Wh^2} \quad (1)$$

where W is the channel width, h is the channel height, and Q is the volumetric flow rate.

After developing, the master is coated with trichloro(1*H*,1*H*,2*H*,2*H*-perfluorooctyl)silane. Polydimethylsiloxane (PDMS) (Sylgard 184) is prepared with a 10 : 1 ratio of the PDMS oligomer and crosslinker and poured onto the master. PDMS is cured at 70 °C for 2 h. Devices are cut out and bonded to clean coverslips (Thermo scientific, 3318) washed with acetone, IPA and dried with nitrogen, using a Harrick oxygen plasma cleaner. To ensure consistent surface properties between runs, bonded devices are stored overnight. The bonded devices and all tubing are autoclaved prior to use.

Microfluidic sterilization and surface modification

Sterile devices and tubing are initially filled with 70% ethanol to ensure complete wetting in hydrophobic chambers. Inlet and exit tubings are connected to device using 20-gauge blunt tip needles (acetone is used to remove needle from Luer lock fittings). Length of inlet tubing is held constant between runs. Ethanol is immediately rinsed from device with DI water (SBS-functionalized surfaces) or 1× PBS (glass surfaces). To functionalize device surface, 10 mg mL^{-1} SBS solution is flowed into device and allowed to equilibrate on surface 1 hour. Surface is then rinsed with DI water followed by 1× PBS.

Bacteria adhesion, growth and removal

Chambers are inoculated with diluted bacteria solution in LB Media (0.5 mL overnight culture in 10 mL fresh LB media). Bacteria solution is flowed through the device in significant volume to fully rinse the PBS from the device, the flow is then stopped for a predetermined amount of time (''pause time'' below) followed by rinsing with 1 mL LB Media at a volumetric flow rate of 1 mL min^{-1} to remove weakly adhered bacteria from the inlet tubing. Following this rinsing step, flow is stopped. Surfaces are then imaged use a Nikon DiaPhot300 microscope with a 40× objective.

A 0.2 μm sterile syringe filter is placed in line near the fluid inlet to prevent bacteria from swimming upstream into fresh media. Inoculation and initial rinsing conditions are identical to those in the adhesion experiment except for after the initial 1 mL min^{-1} rinse for 1 min the flow is reduced to 1 μL min^{-1}. For bacteria growth experiments images are taken every 15 s for 3–4 hours until in-focus bacteria density reaches the point that the tracking code can no longer follow individual bacteria. The rate of this growth is tracked using a tracking code in Python based on the trackpy package. After 4 hours of initial observation the biofilms are placed in a 37 °C incubator overnight.

After 24 hours of growth (from the time of initial inoculation) established biofilms are subject to a rinsing challenge. The rinsing challenge consists of flowing PBS at 1 mL min^{-1} for 1 min and observing the effects of the rinsing on the biofilm.

Live/dead staining and confocal microscopy

Glass and SBS-functionalized devices subjected to rinsing challenge are stained by a live/dead BacLight bacterial viability kit (Thermo Fischer). A staining solution containing a final concentration of 3.34 μM Syto9 and 20 μM propidium iodide are prepared in PBS and flowed through the devices at a 10 μL min^{-1} flow rate for 40 min in the dark. Devices are imaged with a Stellaris confocal microscope (Leica) for green (500–550 nm) and red (590–650 nm) signals corresponding to live and dead populations at the bottom surface. The resulting single channel grey-scale images are quantified for the number of fluorescent cells using FIJI ''find maxima'', which identifies and quantifies pixels with a local maximal intensity, signifying a fluorescently stained cell. The threshold is set at 25. The percentage of live bacteria is calculated as the percentage of live-stained cells divided by the total-stained cells that are at the surface at the

time of imaging. Data collected from the widest zone of the microfluidics device (shear rate at 10^4 s^{-1}) from three experiments.

Results and discussion

Surface functionalization and characterization

We first establish the protocol for modifying glass with (3-(dimethyl;(3-trimethoxysilyl)propyl)ammonia propane-1-sulfonate) (a sulfobetaine silane, or SBS, Mw 329.5). Glass, a commonly used surface for bacteria adhesion, is used as a control. Previous studies by Knowles *et al.* have shown that the grafting of SBS on glass depends on the pH of the aqueous SBS solution.[37] For this study, an aqueous solution of 31 mM SBS is used to functionalize the glass-PDMS microfluidic device to avoid solvent intrusion of the semi-permeable PDMS. The grafting of the SBS takes place in neutral to slightly acidic conditions (pH $\sim$ 6.8–7.0) to promote the adsorption of individual SBS molecules, rather than SBS oligomers, as illustrated in Fig. 1(A).

The grafting of the SBS onto the glass surface is characterized using QCM-D and streaming potential measurements. As seen in Fig. 1(B), when the SBS solution is flowed over a SiO_2-coated QCM crystal, there is a rapid decrease in the resonance frequency of the crystal as the molecule and surrounding water begin to interact with the silica surface. This initial shift decreases in magnitude and approaches a constant frequency after about 3500 s (58.3 min) as the near surface boundary layer containing water, grafted SBS and adsorbed SBS reaches equilibrium. Covalent bond formation of SBS onto the SiO_2 surface releases methanol which likely contributes to some of the mass loss between 500 s and 3750 s. After 3750 s, the deposited layer is rinsed with DI water. This rinsing step removes the free molecules from the surface leaving a covalently grafted SBS layer of about 30 ng cm^{-2} which corresponds to 0.55 molecules per nm^2, consistent with grafting densities of silanes on silica reported in the literature.[38] This value, however, is lower than the density that can be obtained using other types of silanes such as octadecyltrichlorosilane and dodecyltrichlorosilane which are able to pack densely on the surface, especially when formed using an organic solvent at an elevated temperature.[39–41] The relatively low density obtained with SBS may be due to its bulky head group and the mild reaction condition used for silanization. Streaming potential measurements shown in Fig. S1 (ESI†) also confirm a shift in the isoelectric point of the SiO_2 surface upon modification with SBS.

To test the stability of the covalently grafted SBS on the silica surface, the SBS-treated crystal is subsequently challenged by a phosphate buffered saline (PBS) rinse at ten times the volumetric flow at which SBS is initially deposited. Once equilibrated to the PBS solution, the resonance frequency of the crystal remained constant throughout the 40 min of PBS rinsing, as seen in Fig. 1(B) (shaded yellow), suggesting no loss of mass during this rinse challenge. After switching back to water, the resonance frequency shift equilibrated to the pre-PBS rinsing level at -2 Hz, suggesting that 0.548 molecules per nm^2 of SBS is robustly grafted on the silica crystal. Although the exact grafting density of SBS on the glass surface may be different from that on the silica quartz crystal used for QCM-D characterization, the result from the streaming potential strongly suggests the functionalization on glass indeed changes the surface characteristics drastically.

To confirm the grafting of the zwitterionic group, the thickness of the SBS layer on silicon with a native oxide is measured using an ellipsometer, and the surface topography is characterized using atomic force microscopy (AFM). The thickness of the SBS layer determined by ellipsometry is about 1 nm. AFM shows that the SBS-functionalized surface is rougher than the unfunctionalized surface. As seen in Fig. 2, the root mean square roughness (R_q) of the uncoated silicon wafer is about 0.13 nm, whereas the R_q of the SBS-coated coated silicon wafer is about 0.43 nm. In Fig. S2(ESI†), R_q of the uncoated glass and SBS-coated glass are about 0.14 nm and 0.31 nm, respectively. The roughness of silicon wafers is lower than on glass surfaces. Because of the surface roughness of the glass, it is likely that the absolute density of SBS is different from that on the Si wafer. However, we use a Si wafer as the model substrate to obtain an accurate measure of the silane thickness. Similar to the silicon case, the SBS-functionalized glass surface is rougher

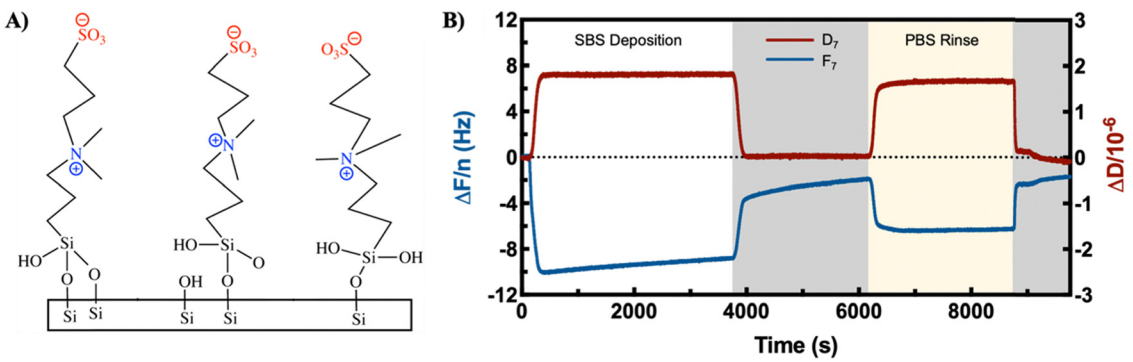

Fig. 1 (A) Grafting of SBS on glass surface. (B) QCM-D results for the adsorption of the SBS onto a silica-coated QCM crystal. Shaded grey areas indicate where DI water is flowing, the yellow area indicates a rinse challenge using phosphate buffered saline, and the white area represents exposure to a solution containing SBS. For clarity only the 7th overtone is shown; other overtones behaved similarly.

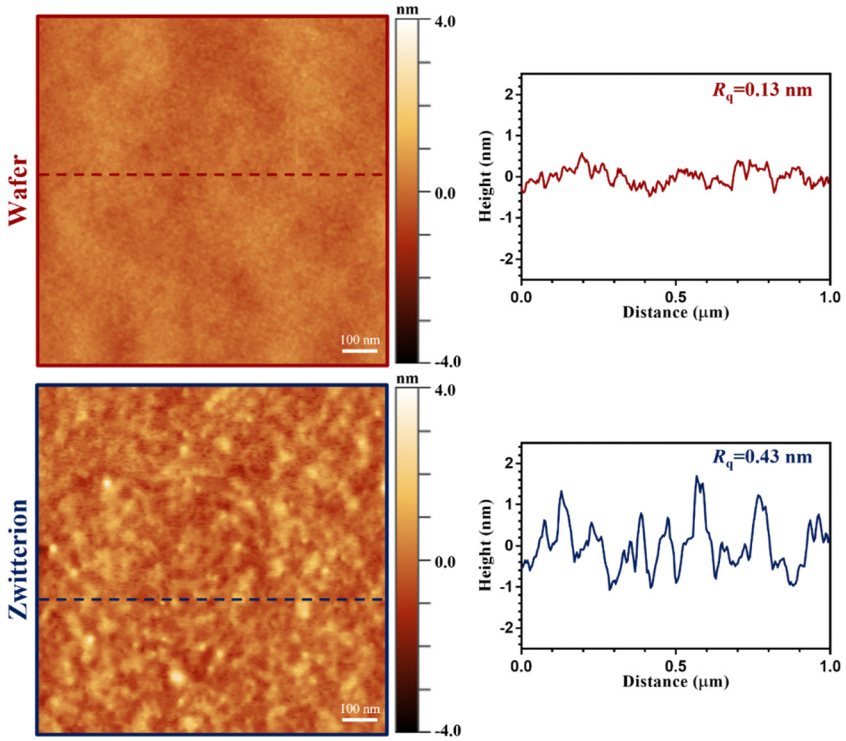

Fig. 2 Comparison of control and SBS-functionalized surfaces measured by atomic force microscopy(AFM). The height profiles for the corresponding lines are drawn in AFM images (dashed lines). The root mean square roughness (R_q) in the line scans was measured over a 1-micron × 1 micron area.

than the initial glass surface. The relatively higher surface roughness likely indicates that SBS molecules form a heterogenous layer with tightly packed and loosely packed regions possibly presenting defects. We do not believe this is a major concern, however, because our focus is to study how surface-grafted zwitterionic groups affects the removal of bacteria from the surface under shear even if the coating is imperfect. By comparison, one would expect a completely dense packed SBS coating (only possible on a model surface) to better resist bacteria adhesion.

Antifouling tests using a protein

A widely adopted benchmark test for rapid screening of biofouling on a surface is to measure how much the surface resists protein adhesion.[42] We characterize the adsorption of bovine serum albumin (BSA, 66 kDa) onto glass and SBS-modified glass surfaces using QCM-D. BSA is used as a surface passivating agent because of its ability to adsorb strongly onto a wide variety of surfaces, serving as an ideal biofoulant. Although BSA carries a net negative charge, the presence of positively charged lysine residues and the resulting heterogeneity of the surface charge allows it to adhere to surfaces with negative surface charge such as glass.[43] Both the glass and the SBS-functionalized surfaces are exposed to a 1 mg mL^{-1} BSA solution. Fig. 3 shows fundamental differences in how BSA interacts with the glass surface compared to an SBS-functionalized surface. On the glass, a gradual decrease in frequency (F) is observed simultaneously with an increase in dissipation (D) indicating BSA adsorption on the surface. After rinsing with PBS (starting around

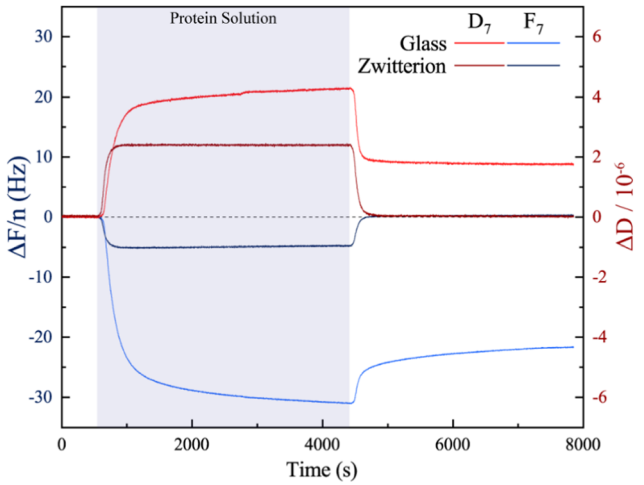

Fig. 3 QCM-D showing the resistance to BSA adsorption on glass and SBS-functionalized surfaces. After rinsing all the protein is removed from the SBS-functionalized surface. Gray and white regions represent exposure to BSA solution and PBS, respectively. Only the 7th overtone is shown for clarity.

4400 s), the frequency increases to a plateau and the dissipation decreases, corresponding to approximately 350 ng cm^{-2} of BSA remains on the glass. Similarly, on the SBS-functionalized surface there is a rapid increase of dissipation and decrease of frequency likely attributed to the change in the viscosity of the solution and weak adsorption of BSA, respectively. However, both the frequency and the dissipation return to the initial values upon rinsing with

PBS, indicating that few proteins remain adhered on the SBS-functionalized surface.

The complete removal of adsorbed BSA on SBS-modified surfaces is likely due to the strong interactions between water and the zwitterionic SBS molecules. Specifically, the strong polarity of the zwitterionic head group with two oppositely charged groups leads to very tight binding of water molecules to the surface. In order for the proteins to adhere to the surface, these water molecules must be displaced which is thought to be energetically unfavorable.[44,45] This lack of ability for the proteins to displace the water molecules leads to a higher fouling resistance for SBS-modified surfaces compared to other chemistries such as PEG-based brushes and hydrogels.

Flow chamber design and flow profiles

Flow chambers, such as drip-flow reactors and parallel plate flow cells, provide constant nutrient flow and an opportunity to study various aspects of biofilm physiology, such as its development,[46] biofilm antibiotic tolerance,[47,48] and the effect of shear on initial bacteria adhesion to a surface.[49] Microfluidic flow chambers, with their smaller length scale, provide a powerful method to miniaturize and rapidly screen surfaces.[50–52] The device used in this study is designed to monitor the early stage of bacteria adhesion on a surface, the growth of those bacteria into microcolonies and biofilms, and more importantly, their subsequent removal under different flow conditions. A simple one channel with five shear zones of varying width is designed to allow bacteria to be exposed to five different shear conditions in one device as shown in Fig. 4(A).

As summarized in Table 1, shear rates calculated using a model fluid, with the viscosity of 10^{-3} Pa s and a density of 0.997 g cm^{-3} at the flow rates of 1 and 1000 μL min^{-1} through a rectangular channel, generating physiologically relevant shear rates ranging from 10 s^{-1} to 100 000 s^{-1}.

The flow profiles in the five different zones of the channel are also calculated using computational fluid dynamic modeling (Fluid Flow Fluent Pack in Workbench 19 r2). The wall shear rate profile for the entry portion of the channel at 1 μL min^{-1} is shown in Fig. 4(B). The maximum shear rate (shear rate at wall in the center of the channel) along with the calculated average shear rate is shown in Table 1. Consistent with common understandings in fluid mechanics, the channel walls have a lesser effect on the overall flow behavior in wide channels than in narrow channels, resulting in maximum shear rates almost identical to that of the calculated average shear rate in zone 5.

Table 1 Shear rates in different flow zones of the microfluidic device employed in this study

		Shear rate at 1 mL min^{-1} (s^{-1})	Shear rate at 1 μL min^{-1} (s^{-1})	
Zone	Channel width (μm)	Calculated	Calculated	Max in CFD Model
1	100	100 000	100	151.9
2	200	50 000	50	64.7
3	400	25 000	25	28.2
4	600	16 700	16.7	17.7
5	1000	10 000	10	10.3

Initial bacteria adhesion

We use the five-zone microfluidic device to study the initial adhesion of bacteria. Both the glass and the SBS-functionalized surfaces are exposed to bacteria from the same initial culture which ensures consistency in the growth phase and concentration. The flow of bacteria suspension through the microfluidic device is paused for 15 min to allow bacteria to explore the surfaces; subsequently, the microfluidic channel is rinsed with PBS at the flow rate of 1 mL min^{-1}. Fig. 5(A) shows representative images for the highest and lowest rinsing shear rates on both surfaces at a pause time of 15 min. Fig. 5(B) shows the coverage of cells as shear rate increases from 10 000 to 100 000 s^{-1} on glass and the SBS-functionalized surfaces. Two trends are observed. First, for both surfaces, fewer cells remain adhered on surfaces as the shear rate increases. This observation indicates that the range of shear rates giving measurable changes in cell coverage has been determined. Secondly, more bacteria remain on the glass surface than on

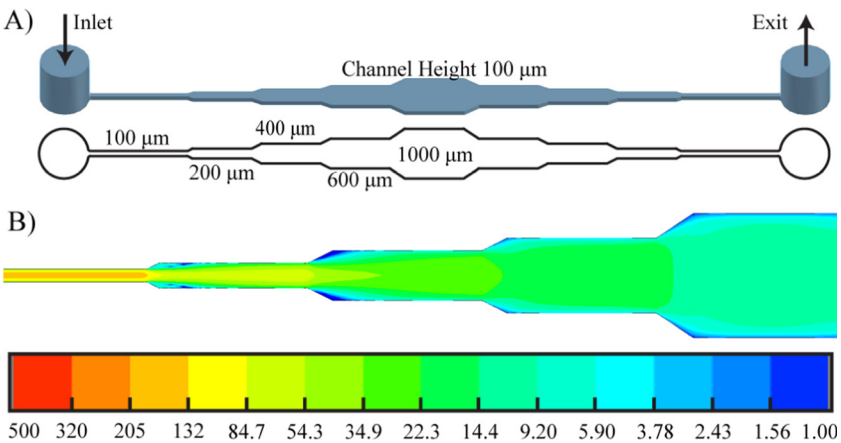

Fig. 4 (A) Design of the microfluidic device. (B) Shear rates (s^{-1}) on the wall of the chamber as calculated using computational fluid dynamic modeling (CFD).

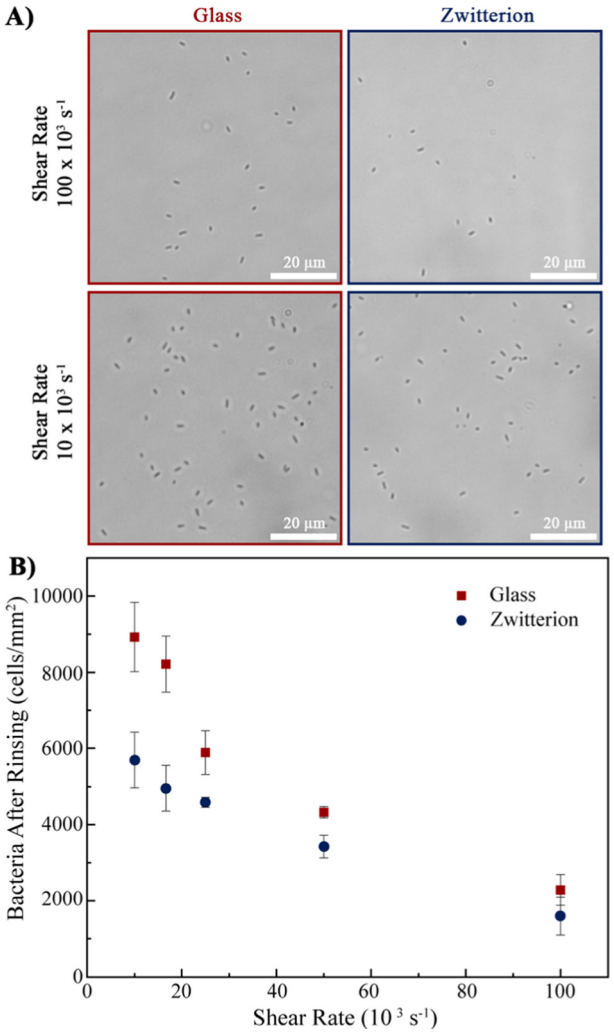

Fig. 5 (A) Representative images showing bacteria coverage on respective surfaces at the lowest and highest shear rates at a pause time of 15 min. (B) Bacteria retained on surface after rinsing with a pause time of 15 min. The surface is rinsed with PBS for 1 min at 1 mL min^{-1}. Fewer bacteria retained on the SBS-functionalized surface under all tested shear rates, with the greatest difference of approximately 40% less retained at the lowest shear rate of 10 000 s^{-1}. Error bars represent standard deviation.

the SBS-functionalized surface in all shear zones as shown in Fig. 5(B). Compared to an SBS-functionalized surface, a glass surface has up to 40% more bacteria retained at the lowest tested shear rate of 10 000 s^{-1}. The difference between the glass and the SBS-functionalized surface decreases as shear rate increases, suggesting a high shear rate becomes the dominating factor of bacteria removal regardless of the underlying bacteria-surface interaction. Although the SBS-functionalized surface exhibits strong resistance to BSA adsorption, as seen in Fig. 3, some bacteria remained adhered to the SBS-functionalized surface after rinse, as seen in Fig. 5(B), even though the duration of pre-rinsing bacteria-surface interaction (15 min) is less than the exposure time of the protein in the anti-fouling test (~40 min). This observation is consistent with previous reports where bacteria are still able to adsorb onto zwitterionic surfaces that are resistant to various proteins including human serum albumin and fibrinogen.[24,53,54] However, the interaction between a surface modified with zwitterionic groups and a bacterium can be as weak as that predicted by the DLVO theory.[53] Also, the adhesion of bacteria to the BSA-resistant surface reflects that bacteria may be able to take advantage of surface defects to initiate adhesion. Imperfect coverage likely allows for some portions of the surface to have nanoscale pinholes and defects with lower density of the zwitterionic SBS molecules. In this study the coverage of SBS molecules can be less homogeneous than the typical coverage of silanol groups on glass.[55] When bacteria have time to sense and sample the surface they can adhere to these areas. It is also important to keep in mind the interplay of various aspects of the near-field bacteria-surface interaction,[56–59] which has much more complexity, partly due to the bacterial surface appendages and swimming dynamics, than that of a single globular protein such as BSA. It is likely the SBS functionalization changed physiochemical details such as the steric and electrostatic interactions, friction, and hydrophobicity, resulting in a gross outcome of less adhesion and easier removal of bacterial cells.

The effect of pause time is investigated by varying the amount of time between the initial bacteria inoculation and the rinsing step. Pause times of 0 (<30 s), 15, 30 min and 1 hour are studied. Representative images for no pause and 15 min (at a shear rate of 16 700 s^{-1}) are shown in Fig. 6(A). As quantified in Fig. 6(B), bacteria adhered to both surfaces within the first 15 minutes of inoculation, with 2000 cell per cm^2 at 0 min on both surfaces to roughly 8000 cell per cm^2 on glass and 5000 cell per cm^2 on SBS-functionalized surface at 15 min. After the initial 15 min, however, we do not observe a significant difference when the time doubles or quadruples. These results indicate that the transition between the initial stage of reversible attachment to more avid adhesion occurs on the time scale of a few minutes and is completed by the 15 min time point.

Bacteria growth

After their initial adhesion, bacteria begin to grow and divide on the surface. The growth curves and representative images of the surfaces at various time points are shown in Fig. 7(A) and Fig. S3(ESI†), respectively. Both curves show similar behavior where the bacteria density initially does not change. During this time bacteria are in a lag phase, adapting to the surface.[60] During this time the daughter cells of the few bacteria that undergo division do not adhere to the surface. At this point there is likely insufficient amounts of EPS secreted to keep the bacteria adhered to the surface in the presence of the flow. As bacteria continue to divide on the surface, more EPS is secreted, trapping more bacteria in the near surface region. Exponential growth phase starts around 97.8 min and 131.5 min (after the rinse) for glass and SBS-functionalized surface, respectively. Due to slight drifts in the baseline, to compare the lag times on the normalized graph it is important to look not at the time when the counts begin to increase from the baseline but the time when the counts complete the first doubling. Considering that the doubling time of *P. aeruginosa*

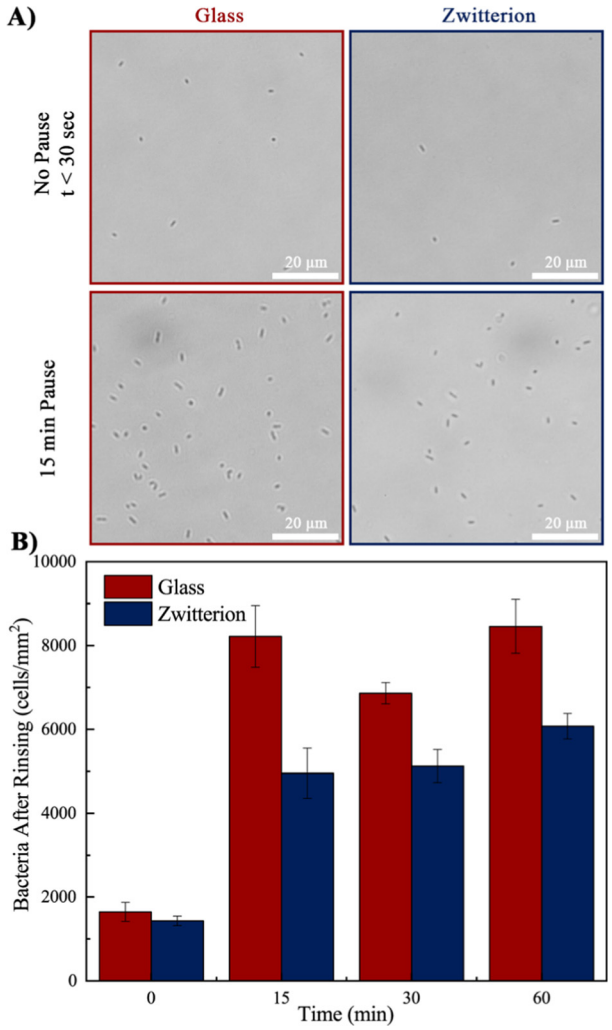

Fig. 6 (A) Representative images showing the initial adhesion with varying pause times (the time between inoculation and rinsing) on control and SBS-functionalized surfaces at a shear rate of 16 700 s^{-1}. (B) Quantification of bacteria retained on surface after rinsing with varying pause times of 0–60 min. Error bars represent standard deviation. The antifouling behavior of the zwitterionic SBS-functionalized surface causes less bacteria to adhere in a given time frame.

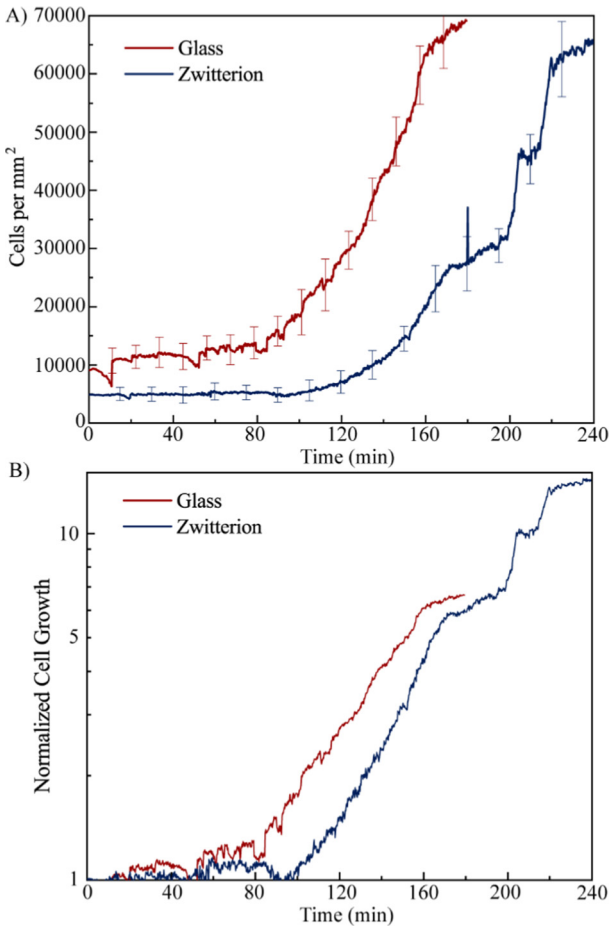

Fig. 7 Number of bacteria near the surface as a function of time in both the absolute numbers (A) which are affected by the initial seeding density and normalized counts (B).

in LB media is about 25–35 minutes[61,62] this difference is significant (at least 1 generation). During the exponential growth phase, the bacteria divide at a faster rate while staying near the surface. The resulting daughter cells may also adhere to the surface, or they may be rinsed away in the media. With more daughter cells remaining on the surface, individual bacteria grow into microcolonies, and eventually biofilms start to develop on the surfaces.

Although less bacteria adhere to the SBS-functionalized surface compared to the control surface, when growth enters the exponential phase, the growth rates on the two surfaces are similar, as indicated by the similar slopes of the growth curves during exponential phase in Fig. 7(A). When we inoculate a more concentrated culture to the SBS-functionalized device, both surfaces can achieve similar initial cell densities, as shown in Fig. S3 (ESI†). When the number of bacteria on the surface is normalized based on the number of bacteria initially on the surface, the bacteria growth on the surfaces are very similar to one another as shown in Fig. 7(B). However, the SBS-functionalized surfaces have a longer lag phase, as seen in growth curves in Fig. 7 and representative images of bacteria at various timepoints on both surfaces in Fig. S4 (ESI†). This indicates that it takes more time for the fewer bacteria accumulated on the SBS-functionalized surface to adjust to growth on the zwitterionic surface or to secrete sufficient amounts and varieties of EPS to induce adhesion of daughter cells. This may indicate that once the biofilm and EPS start to form the interactions and growth of bacteria are mainly affected by biofilm itself and not the underlying surface.

Removal of bacteria under flow

We study the further growth of bacteria and their removal on these surfaces by placing the microfluidic devices in a 37 °C incubator overnight and subsequently subjecting them to an external shear. After 24 hours, biofilms with dense layers of bacteria are observed on both surfaces. These biofilms are subjected to a rinsing challenge by flowing PBS at a flow rate of 1 mL min^{-1} for 3 min which induces shear rates from

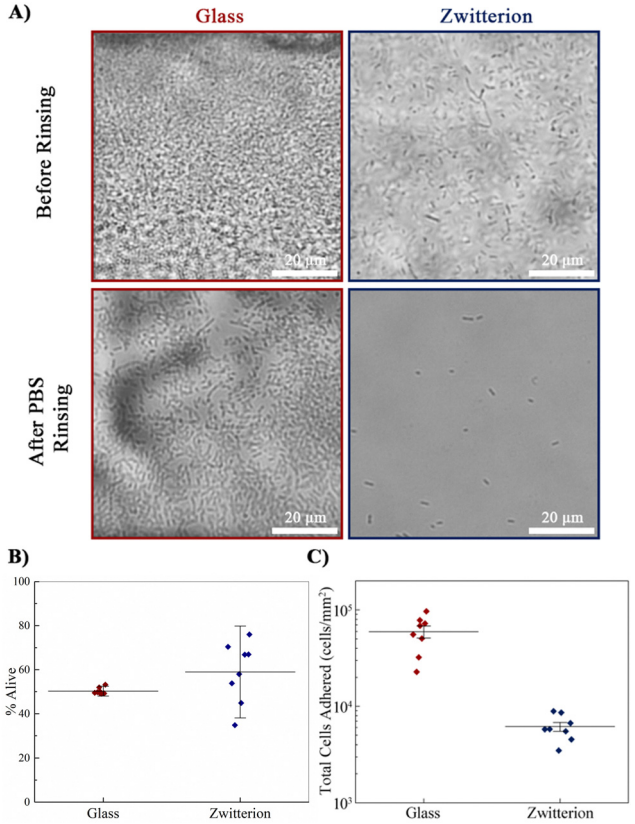

Fig. 8 (A) Images of biofilm after 24 hour growth in the microfluidic device before and after rinsing with PBS at the flow rate of 1 mL min^{-1}. (B) Percentages of live over total near surface bacteria after a rinse challenge as quantified by live/dead BacLight staining and confocal microscopy. (C) Number of total near surface bacteria after a rinse challenge at the shear rate of 10^4 s^{-1} on the glass and the SBS-functionalized surfaces.

10 000 and 100 000 s^{-1} in the 5-zone microfluidic device. After rinsing, the majority of the biofilm is removed from the zwitterionic surface whereas approximately 10-fold more of surface bacteria remained on the glass surface, as seen qualitatively in Fig. 8(A) and Fig. S5 (ESI†) and quantitatively in Fig. 8(C). Intriguingly, as seen in Fig. 8(B), the percentages of cells that are alive following the rinse challenge remain similar in both devices, as quantified by a live/dead BacLight staining assay, followed by image analysis as described in Methods and shown in Fig. S6 (ESI†). These results indicate that although the SBS-functionalized surface is not exerting an intrinsic biocidal effect there is a significant difference in how the bacteria adhere to the zwitterionic surface. We attribute this difference to the underlying surface chemistry which can have a significant impact on the avidity of bacteria adhesion to the surface and in turn the susceptibility of bacteria to shear-induced removal.

Conclusions

In this work, we have used a multi-shear zone microfluidic device to study the differences in the initial adhesion, growth, viability, and removal of bacteria on glass and SBS-functionalized surfaces. The zwitterionic surface based on SBS exhibit excellent BSA resistance. Although smaller numbers of bacteria adsorb onto the zwitterionic group modified surface initially, bacteria are eventually able to attach and grow on such a surface. Despite the ability to resist and weaken bacteria adhesion, the viability of bacteria is not compromised by dwelling and growing on the zwitterionic surface. However, subsequent rinsing of the surface under flow shows that bacteria on the SBS-functionalized surface are more easily removed, indicating that such a treatment can facilitate bacteria removal in the initial stages of biofilm development. Our study suggests that one potential benefit of zwitterionic surface groups is facilitating the removal of bacteria under shear from the surface to prevent the formation of fully mature and robust biofilms. While this study focused on the effect of surface chemistry on the removal of bacteria from the surface under flow, there are several additional factors such as surface roughness and stiffness that could potentially influence the avidity of bacteria adhesion on the surface. The microfluidic platform introduced in this work provides a high throughput and rapid method of investigating the effect of these factors on the removal of bacteria in the initial and potentially later stages of biofilm formation. Moreover, our approach can be further extended to study the effect of the surface on the susceptibility of bacteria and biofilms to biocides. While our study focused on testing the feasibility of detaching and removing bacteria from zwitterion functionalized surfaces, there are other factors that must be addressed in future studies. For example, the attachment of bacteria and the growth of biofilms have been closely correlated with the production and incorporation of EPS in the biofilms. To understand the mechanism behind the observation we report in this study, detailed studies of the interactions between EPS and zwitterionic groups and the effect of shear on their interactions are necessary. Moreover, studies of the effectiveness of zwitterionic groups on the removal of other types of bacteria would more generalize the impact of this work.

Conflicts of interest

There are no conflicts to declare.

Acknowledgements

This work was supported by COMPASS (Complex Assemblies of Soft Matter). The authors would like to acknowledge primary support from MRSEC-DMR-1720530. We also thank Sasha Zavgorodnya and Christopher O'Bryan for their technical support.

References

1 W. B. Whitman, D. C. Coleman and W. J. Wiebe, *Proc. Natl. Acad. Sci. U. S. A.*, 1998, **95**, 6578–6583.
2 H. H. Tuson and D. B. Weibel, *Soft Matter*, 2013, **9**, 4368–4380.

3 J. C. Conrad and R. Poling-Skutvik, *Annu. Rev. Chem. Biomol. Eng.*, 2018, **9**, 175–200.
4 U. Römling, S. Kjelleberg, S. Normark, L. Nyman, B. E. Uhlin and B. Åkerlund, *J. Intern. Med.*, 2014, **276**, 98–110.
5 R. D. Wolcott, D. D. Rhoads, M. E. Bennett, B. M. Wolcott, L. Gogokhia, J. W. Costerton and S. E. Dowd, *J Wound Care*, 2010, **19**, 45–46, 48-50, 52-43.
6 J. A. Fernandes, L. Santos, T. Vance, T. Fileman, D. Smith, J. D. D. Bishop, F. Viard, A. M. Queirós, G. Merino, E. Buisman and M. C. Austen, *Mar. Policy*, 2016, **64**, 148–155.
7 C. C. C. R. de Carvalho, *Front. Mar. Sci.*, 2018, **5**, 126.
8 T. R. Bott, *Appl. Therm. Eng.*, 1998, **18**, 1059–1066.
9 E. Zimlichman, D. Henderson, O. Tamir, C. Franz, P. Song, C. K. Yamin, C. Keohane, C. R. Denham and D. W. Bates, *JAMA Intern. Med.*, 2013, **173**, 2039–2046.
10 CDC, 2013, 114.
11 K. N. Stevens, S. Croes, R. S. Boersma, E. E. Stobberingh, C. van der Marel, F. H. van der Veen, M. L. Knetsch and L. H. Koole, *Biomaterials*, 2011, **32**, 1264–1269.
12 K. S. Huang, C. H. Yang, S. L. Huang, C. Y. Chen, Y. Y. Lu and Y. S. Lin, *Int. J. Mol. Sci.*, 2016, **17**, 1578.
13 K. W. Kolewe, S. R. Peyton and J. D. Schiffman, *ACS Appl. Mater. Interfaces*, 2015, **7**, 19562–19569.
14 K. W. Kolewe, K. M. Dobosz, T. Emrick, S. S. Nonnenmann and J. D. Schiffman, *ACS Appl. Bio Mater.*, 2018, **1**, 33–41.
15 K. W. Kolewe, S. Kalasin, M. Shave, J. D. Schiffman and M. M. Santore, *ACS Appl. Mater. Interfaces*, 2019, **11**, 320–330.
16 X. Yu, W. Yang, Y. Yang, X. Wang, X. Liu, F. Zhou and Y. Zhao, *J. Mater. Sci.*, 2020, **55**, 14544–14557.
17 D. Perera-Costa, J. M. Bruque, M. L. González-Martín, A. C. Gómez-García and V. Vadillo-Rodríguez, *Langmuir*, 2014, **30**, 4633–4641.
18 X. Xun, Y. Wan, Q. Zhang, D. Gan, J. Hu and H. Luo, *Appl. Surf. Sci.*, 2020, **505**, 144566.
19 F. L. Game, R. J. Hinchliffe, J. Apelqvist, D. G. Armstrong, K. Bakker, A. Hartemann, M. Löndahl, P. E. Price and W. J. Jeffcoate, *Diabetes/Metab. Res. Rev.*, 2012, **28**(Suppl 1), 119–141.
20 F. Pietsch, A. J. O'Neill, A. Ivask, H. Jenssen, J. Inkinen, A. Kahru, M. Ahonen and F. Schreiber, *J. Hosp. Infect.*, 2020, **106**, 115–125.
21 K. Vasilev, J. Cook and H. J. Griesser, *Expert Rev. Med. Devices*, 2009, **6**, 553–567.
22 S. Lowe, N. M. O'Brien-Simpson and L. A. Connal, *Polym. Chem.*, 2015, **6**, 198–212.
23 Z. Zhang, S. Chen, Y. Chang and S. Jiang, *J. Phys. Chem. B*, 2006, **110**, 10799–10804.
24 G. Cheng, Z. Zhang, S. Chen, J. D. Bryers and S. Jiang, *Biomaterials*, 2007, **28**, 4192–4199.
25 I. C. Saldarriaga Fernández, H. C. van der Mei, M. J. Lochhead, D. W. Grainger and H. J. Busscher, *Biomaterials*, 2007, **28**, 4105–4112.
26 A. K. Epstein, T.-S. Wong, R. A. Belisle, E. M. Boggs and J. Aizenberg, *Proc. Natl. Acad. Sci. U. S. A.*, 2012, **109**, 13182–13187.
27 G. O'Toole, H. B. Kaplan and R. Kolter, *Annu. Rev. Microbiol.*, 2000, **54**, 49–79.
28 D. Davies, *Nat. Rev. Drug Discovery*, 2003, **2**, 114–122.
29 H. C. Flemming and J. Wingender, *Nat. Rev. Microbiol.*, 2010, **8**, 623–633.
30 P. Shivapooja, Q. Wang, B. Orihuela, D. Rittschof, G. P. López and X. Zhao, *Adv. Mater.*, 2013, **25**, 1430–1434.
31 T. O'Loughlin Colleen, C. Miller Laura, A. Siryaporn, K. Drescher, F. Semmelhack Martin and L. Bassler Bonnie, *Proc. Natl. Acad. Sci. U. S. A.*, 2013, **110**, 17981–17986.
32 S. Lecuyer, R. Rusconi, Y. Shen, A. Forsyth, H. Vlamakis, R. Kolter and H. A. Stone, *Biophys. J.*, 2011, **100**, 341–350.
33 P. Thomen, J. Robert, A. Monmeyran, A.-F. Bitbol, C. Douarche and N. Henry, *PLoS One*, 2017, **12**, e0175197.
34 V. Yadav, Y. A. Jaimes-Lizcano, N. K. Dewangan, N. Park, T.-H. Li, M. L. Robertson and J. C. Conrad, *ACS Appl. Mater. Interfaces*, 2017, **9**, 44900–44910.
35 B. F. Gilmore, T. M. Hamill, D. S. Jones and S. P. Gorman, *J. Biomed. Mater. Res., Part B*, 2010, **93**, 128–140.
36 M. A. Jacobs, A. Alwood, I. Thaipisuttikul, D. Spencer, E. Haugen, S. Ernst, O. Will, R. Kaul, C. Raymond, R. Levy, L. Chun-Rong, D. Guenthner, D. Bovee, M. V. Olson and C. Manoil, *Proc. Natl. Acad. Sci. U. S. A.*, 2003, **100**, 14339–14344.
37 B. R. Knowles, P. Wagner, S. Maclaughlin, M. J. Higgins and P. J. Molino, *ACS Appl. Mater. Interfaces*, 2017, **9**, 18584–18594.
38 S. Gam, J. S. Meth, S. G. Zane, C. Chi, B. A. Wood, K. I. Winey, N. Clarke and R. J. Composto, *Soft Matter*, 2012, **8**, 6512–6520.
39 I. M. Tidswell, T. A. Rabedeau, P. S. Pershan, S. D. Kosowsky, J. P. Folkers and G. M. Whitesides, *J. Chem. Phys.*, 1991, **95**, 2854–2861.
40 H.-G. Steinrück, A. Schiener, T. Schindler, J. Will, A. Magerl, O. Konovalov, G. Li Destri, O. H. Seeck, M. Mezger, J. Haddad, M. Deutsch, A. Checco and B. M. Ocko, *ACS Nano*, 2014, **8**, 12676–12681.
41 J. M. Castillo, M. Klos, K. Jacobs, M. Horsch and H. Hasse, *Langmuir*, 2015, **31**, 2630–2638.
42 N. Tufenkji and M. Elimelech, *Langmuir*, 2005, **21**, 841–852.
43 K. Kubiak-Ossowska, B. Jachimska and P. A. Mulheran, *J. Phys. Chem. B*, 2016, **120**, 10463–10468.
44 C. Leng, S. Sun, K. Zhang, S. Jiang and Z. Chen, *Acta Biomater.*, 2016, **40**, 6–15.
45 J. B. Schlenoff, *Langmuir*, 2014, **30**, 9625–9636.
46 L. Ma, D. Jackson Kara, M. Landry Rebecca, R. Parsek Matthew and J. Wozniak Daniel, *J. Bacteriol.*, 2006, **188**, 8213–8221.
47 J. Liao and K. Sauer, *J. Bacteriol.*, 2012, **194**, 4823–4836.
48 S. Stewart Philip, J. Franklin Michael, S. Williamson Kerry, P. Folsom James, L. Boegli and A. James Garth, *Antimicrob. Agents Chemother.*, 2015, **59**, 3838–3847.
49 P. Alves, J. M. Moreira, J. M. Miranda and F. J. Mergulhão, *Antibiotics*, 2020, **9**, 421.
50 A. Grünberger, C. Probst, S. Helfrich, A. Nanda, B. Stute, W. Wiechert, E. von Lieres, K. Nöh, J. Frunzke and D. Kohlheyer, *Cytometry, Part A*, 2015, **87**, 1101–1115.

51 A. Grünberger, N. Paczia, C. Probst, G. Schendzielorz, L. Eggeling, S. Noack, W. Wiechert and D. Kohlheyer, *Lab Chip*, 2012, **12**, 2060–2068.
52 C. E. M. Krämer, W. Wiechert and D. Kohlheyer, *Sci. Rep.*, 2016, **6**, 32104.
53 C. Rodriguez-Emmenegger, S. Janel, A. de los Santos Pereira, M. Bruns and F. Lafont, *Polym. Chem.*, 2015, **6**, 5740–5751.
54 G. Li, H. Xue, G. Cheng, S. Chen, F. Zhang and S. Jiang, *J. Phys. Chem. B*, 2008, **112**, 15269–15274.
55 M. H. Lee, D. Boettiger, P. Ducheyne and R. J. Composto, *Silanes and Other Coupling Agents*, 2020, **4**, 163–178.
56 H. H. M. Rijnaarts, W. Norde, J. Lyklema and A. J. B. Zehnder, *Colloids Surf., B*, 1999, **14**, 179–195.
57 K.-T. Wu, Y.-T. Hsiao and W.-Y. Woon, *Phys. Rev. E*, 2018, **98**, 052407.
58 C. N. Dominick and X.-L. Wu, *Biophys. J.*, 2018, **115**, 588–594.
59 M. Qi, X. Gong, B. Wu and G. Zhang, *Langmuir*, 2017, **33**, 3525–3533.
60 A. R. Rice, M. A. Hamilton and A. K. Camper, *Microb. Ecol.*, 2000, **40**, 8–15.
61 A. E. LaBauve and M. J. Wargo, *Curr. Protoc. Microbiol.*, 2012, **25**, 6E.1.1–6E.1.8.
62 J. Lin, J. Cheng, K. Chen, C. Guo, W. Zhang, X. Yang, W. Ding, L. Ma, Y. Wang and X. Shen, *Front. Cell. Infect. Microbiol.*, 2015, **5**, 70.

